SANDIA REPORT

SAND98–8246
Unlimited Release
Printed October 1998

TEPIC – A New High Temperature Structural Foam

L. L. Whinnery, S. H. Goods, M. L. Tootle, and C. L. Neuschwanger

Prepared by
Sandia National Laboratories
Albuquerque, New Mexico 87185 and Livermore, California 94550

Sandia is a multiprogram laboratory operated by Sandia Corporation, a Lockheed Martin Company, for the United States Department of Energy under Contract DE-AC04-94AL85000.

Sandia National Laboratories

Issued by Sandia National Laboratories, operated for the United States Department of Energy by Sandia Corporation.

Available to DOE and DOE contractors from
Office of Scientific and Technical Information
P.O. Box 62
Oak Ridge, TN 37831

Prices available from (615) 576-8401, FTS 626-8401

Available to the public from
National Technical Information Service
U.S. Department of Commerce
5285 Port Royal Rd
Springfield, VA 22161

NTIS price codes
Printed copy: A03
Microfiche copy: A01

SAND98-8246
Unlimited Release
Printed October 1998

TEPIC - A NEW HIGH TEMPERATURE STRUCTURAL FOAM

L. L. Whinnery
Materials Processing Department

S. H. Goods and M. L. Tootle
Materials Reliability Department

Sandia National Laboratories
P. O. Box 969
Livermore, CA 94551-0969

C. L. Neuschwanger
Hewlett Packard
1501 Page Mill Road, MS 5L-C
Palo Alto, CA 94304-1126

ABSTRACT

The formulation, processing characteristics, microstructure and mechanical properties of a new structural foam, suitable for use at service temperatures up to 200°C, are reported. In each of these respects, the foam is compared to an existing material, called APO-BMI that is currently in use. When these two foams are directly compared, the new foam, called TEPIC, is found to be superior in its mechanical performance.

TEPIC is formulated from a non-carcinogenic isocyanate, a di-functional epoxide, and glass microballoons. Our approach was to combine chemistries known to form thermally stable products. The principal polymerization products are an oxizolidinone produced by the reaction of the isocyanate with the epoxide and isocyanurate rings formed by the trimerization of the isocyanate. Processing has been examined and large-scale production is discussed in detail. Compared to APO-BMI processing, TEPIC processing is facile and economical.

The structure of the foam resembles a traditional rigid polyurethane foam rather than that of the APO-BMI. That is, the foam is comprised of a continuous resin phase rather than weakly bonded glass microballoons. At a density of 0.42 g/cm^3 or greater, maximum pore size in TEPIC was less than 2 mm, as required for the application.

In regard to specific mechanical properties, quasi-static uniaxial testing indicates that the crush strength of TEPIC at both ambient temperature and 200°C substantially exceeds the minimum requirements (6.9 MPa). The tensile strength is greater than that of the APO-BMI material it is intended to replace (APO-BMI). Energy absorption, measured from impact testing, is equivalent to the foam that is currently deployed.

ACKNOWLEDGMENT

The authors would like to thank Craig Henderson for the initial TEPIC formulation and helpful suggestions. We are grateful to George McEachen from Allied Signal FM&T for supplying all of the APO-BMI material. We would also like to thank Pat Keifer, John Tan, Winalee Carter, John Hachman, Eunizelle Balbin, and Jeff Chames for technical assistance and analytical support.

TABLE OF CONTENTS

FIGURES

TEPIC - A NEW HIGH TEMPERATURE STRUCTURAL FOAM

I. INTRODUCTION

Polymeric foams provide structural support in critical locations in a number of nuclear weapons. When service temperatures approaching 200°C are required, only a very limited selection of foams is available. For these high temperature applications (after 1977), a three-phase syntactic foam called Kerimid 601 has been used.[1,2,3] Kerimid 601 consists of a mixture of methylene dianaline (MDA), bismaleimide (BMI) (together forming the resin phase), glass microballoons (GMB) and air. The foam essentially consists of the hollow spheres "glued" together by the resin phase, a bismaleimide. Air is present in the voids between the microballoons and comprises the third phase. When it was discovered that MDA was carcinogenic, replacement foams were sought.

Some time ago, ASFM&T chose APO-BMI as the three-phase syntactic foam to replace Kerimid 601. APO Cure is the diamine reagent that reacts with maleic anhydride to form the BMI linkages. Both carbon microballoons and glass microballoons have been used in APO-BMI formulations.[4,5,6,7,8] Structurally, APO-BMI is quite similar to Kerimid 601. The processing of these APO-BMI foams is moderately complicated and expensive. The resulting foams are also very brittle, particularly in tension, making machining and handling difficult.

While the properties of ABO-BMI are adequate for the designed application, the combination of the processing difficulties, less than optimum mechanical properties and frangibility concerns have driven a new search for a more mechanically robust and easier handling high temperature structural foam. The absolute requirements for this replacement material remain the same as those for APO-BMI and consist of:

I. Minimum compression failure strength of 6.9 MPa (1000 psi) over the temperature range of 25°C to 200°C
II. Maximum density of 0.6 g/cm^3
III. Maximum void size of 2 mm

Obviously, the constituents were required to be non-carcinogenic. It was desired for the new foam to be less brittle than APO-BMI, and be processible and scaleable to large parts. Further, changes in the design of specific structural supports required that the replacement foam be considerably more machineable than APO-BMI.

Our approach was to combine chemistries known to form thermally stable products. We also wanted the structure to resemble a traditional rigid polyurethane foam rather than the APO-BMI structure since a continuous resin phase is known to have superior mechanical properties and machineablity characteristics. The principal constituents are an oxizolidinone produced by the reaction of an isocyanate with an epoxide and isocyanurate rings formed by the trimerization of an isocyanate.[9] Air is mechanically incorporated into the liquid constituents during mixing and GMB are added to increase the modulus and adjust the density. The high temperature structural foam we developed is called TEPIC (the Epoxy PolyIsoCyanurate).

Since mechanical properties were identified as one of the main requirements for the replacement foam, uniaxial tension, compression, and impact properties of TEPIC foams were investigated in detail. Specifically for TEPIC, strength and ductility in both tension and compression were measured under quasi-static test conditions at both room temperature and 200°C. These properties were compared to those of APO-BMI under similar test conditions. The response of both materials to high rate impact were also assessed. Strain rate effects on compressive strength and modulus were also characterized for TEPIC over seven orders of magnitude in strain rate.

II. EXPERIMENTAL

The reactants used in processing TEPIC are listed in Table 1. The specific quantities listed yield a free rise density of 0.42 g/cm^3. These chemicals were used as supplied without further purification.

Table 1. Chemicals, amounts, and producers used in preparation of TEPIC foams.

Chemical	Amount	Chemical Producer
Epon 826	5911 g	Dow Chemicals
DC193	739 g	Dow Chemicals
PAPI-2094	11084 g	Dow Chemicals
GMB 32/4500	2217 g	3M
TMR-3	51 g	Air Products

Processing

TEPIC foam was processed in a manner similar to traditional rigid polyurethane foams. Each of the reactants was added sequentially, with hand stirring using a metal spatula. First, the epoxy resin (Epon 826) and surfactant (DC193) were combined in a 80 liter container (for the quantities listed in Table 1). Next, the isocyanate (PAPI-2094) was stirred into the mixture, followed by the filler (GMB). The GMB can be difficult to fully incorporate into the liquid mix. To aid in its dispersion, the liquid reactants and the GMB were thoroughly mixed with a 4-inch Conn blade for 3-5 minutes. Periodically, the sides

of the container were scraped with a spatula to help further disperse the GMB. The catalyst (TMR-3) was added last and mixing continued on the Conn blade for 1 minute.

This mixture was poured into a mold and allowed to rise and gel over the next 2 hours at room temperature. The mold was then cured in an oven at 130°C overnight. Because the foam requires strength above ambient, an additional curing step was used to increase the Tg. To this end, the foam was removed from the mold and heated with a gradual ramp, to 200°C over 28 hours. The foam was then held for 5 hours before slowly being cooled to room temperature.

The processing conditions described above and the formulation listed in Table 1 yields a foam having a density of 0.42 g/cm^3 and a maximum void size of 2 mm as required by the application. Attempts to achieve lower densities by varying either the ratio of reactants or processing variables resulted in unsatisfactory foam structures and processing characteristics. For example, reducing the density (by additions of water) resulted in the collapse of the foam during gellation and rise. Other attempts to reduce density by increasing the proportion of GMB, yielded a slurry that trapped large air pockets during mixing. The resulting foam had pores substantially greater the 2 mm allowed for the application.

The processing steps for making TEPIC foam parts are summarized below:

1. Add DC193 to Epon 826 – hand stir
2. Add PAPI-2094 – hand stir
3. Add GMB – hand stir
4. Mix thoroughly with Conn blade
5. Add TMR-3 – mix 60 to 90 sec with Conn blade
6. Pour into mold
7. Let stand at ambient temperature for at least 2 hours
8. Cure mold in 130°C oven overnight
9. Unmold foam
10. Post-cure to 200°C with the following temperature profile
    65°C oven for 5-hours.
    ramp to 150°C over 8-hours and hold for 5-hours
    ramp to 180°C over 5-hours and hold for 5-hours
    ramp to 200°C over 5-hours and hold for 5-hours
    slow cool to 65°C in 5-hours and hold for 5-hours

Observations on TEPIC processing

Prior to adding the catalyst, the mixture is stable at room temperature for several hours, but would form a crust if left overnight. This crust is probably due to the isocyanate reacting with moisture in the air. Storing in a nitrogen atmosphere may increase the shelf life of this mixture.

The time interval between Steps 5 and 6 should be less than 2 minutes. If the mix is not transferred into the mold fast enough, it will start to gel in the mixing container.

During the post-cure cycle, Step 10, the actual ramp rate will vary depending on the characteristic part dimension. Parts with thicker dimensions will require slower ramp rates in order to avoid charring. For example, the ramp rate called out in Step 10 was optimized for a part with a maximum thickness of 10 cm.

Mechanical Testing

Uniaxial tension and compression properties of TEPIC were evaluated. All specimens for mechanical testing were machined from a single block of TEPIC having a density of 0.42 g/cm^3. The cylindrical axis of the samples were parallel to the rise direction of the foam. Tension properties were evaluated only at room temperature. The tension specimens had a gage length of 25.4 mm and a reduced gage diameter of 19.0 mm and were bonded to steel pull studs. The reduced gage section insured that failure occurred within the specimen between the attachment points of the extensometer and not at the bondline between the foam and the pull studs. Compression tests were performed at room temperature and 200°C on freestanding right cylinders. For these tests, test specimens measured 28.7 mm (1.13 in) in diameter and 50.8 mm (2.0 in) in length. All tension and compression specimens were instrumented with a mechanically attached extensometer for displacement measurement. Compression and tension specimens are shown in Figure 1.

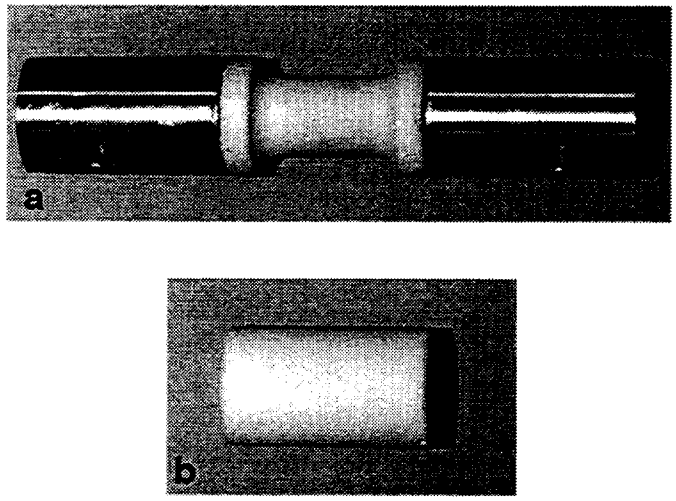

Figure 1. Specimen geometries used in this study. (a) Tension specimen had a 25.4 mm gage length with a 19.0 mm reduced gage diameter. Steel pull studs were bonded to the specimen ends for mounting in the test frame. (b) Compression and impact specimens were simple free standing right cylinders 50.8 mm long and 28.7 mm in diameter.

For tensile testing, modulus (E), ultimate tensile strength (UTS) and energy absorption/unit volume (toughness) were determined. The latter parameter was calculated as the area under the stress-strain curve (see Figure 2). For compression testing,

modulus, crush strength (σ_{cr},) and toughness were determined. These tension and compression properties were compared to those of APO-BMI.

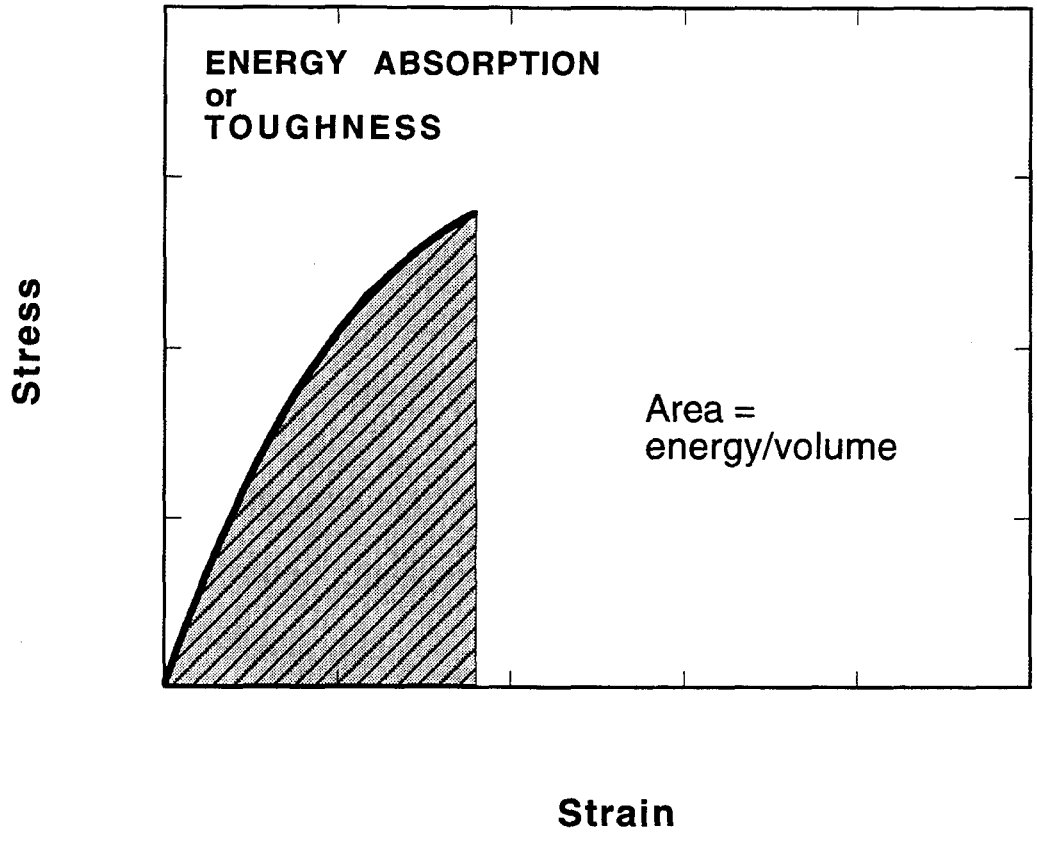

Figure 2. Schematic illustration of the calculation of toughness or energy absorption from either a tension or compression stress-strain curve. The energy absorption is the area under the curve either to the point of failure or to some pre-determined strain value.

The influence of strain rate on modulus and strength of TEPIC was also evaluated at 25°C for specimens tested in compression. For these tests, specimens had the same geometry as those for compression described above, except for the specimens tested at the highest strain rate. For those tests, the specimens were smaller cylinders, measuring 12.7 mm (0.5 in) in both diameter and height.

In order to span the strain rate range of interest, it was necessary to use three different testing instruments. Where possible testing conditions were overlapped so that any systematic differences resulting from the use of the different instruments could be ascertained. Tests at strain rates between 8.3×10^{-6} and 8.3×10^{-3} sec^{-1} were performed on an MTS servomechanical test frame. This instrument is most suited for tests performed at these "quasi-static" strain rates. Higher rate tests, performed at strain rates up to 8.3×10^{-1} sec^{-1}, were run on an MTS servohydraulic test frame. This represented the upper end limitation on strain rate due to both actuator velocity and data acquisition rate. Both of these instruments were operated in "stroke" control mode. In this mode, a

constant displacement rate is imposed on test specimens. All specimens were instrumented with a mechanically attached extensometer for displacement measurement. During each test, load and specimen displacement are monitored and recorded. Stress-strain curves are subsequently generated from these load-displacement data.

The highest strain rate tests were performed on a Dynatup drop weight impact tester. The test frame can be operated in either gravity mode or with pneumatic assist. A high speed data acquisition system, which records the output of an instrumented tup (load cell), has 1 ms resolution and can acquire a complete loading (impact) event in as little as 4 ms. Mechanically attached extensometers cannot be used with this instrument. Rather, crosshead position is measured and recorded during the impact event. This data is then used to compute the strain imposed on a specimen. Tests on TEPIC were performed in gravity mode. Incident velocity of the crosshead corresponded to a strain rate of 200 sec^{-1}. While these are not true constant displacement rate tests, as are the ones described above, analysis of the data revealed that the decrease in velocity during the impact event was less than 5% of the incident value. This same instrument was used to directly compare the impact characteristics of APO-BMI to those of TEPIC.

III. RESULTS AND DISCUSSION

Processing and Structure of Syntactic Foams

APO-BMI

We note that the APO-BMI used in this study was manufactured at ASFM&T. We include the following description of the processing for completeness.

The starting materials and chemistry for APO-BMI are shown in Figure 3. In APO-BMI processing, the reactants (maleic anhydride and APO Cure) are solid powders that are blended with the GMB. This mixture is then poured into a cylindrical mold that can be compacted. The mold is then heated while applying pressure. The heat melts the powder reactants, allowing them to intermix and react. A critical feature of APO-BMI resin is its broad processing window.[4] This results from a large temperature difference between the melting point of the reactants and the initial polymerization temperature. This temperature differential allows the resin to flow as a fluid prior to polymerizing.

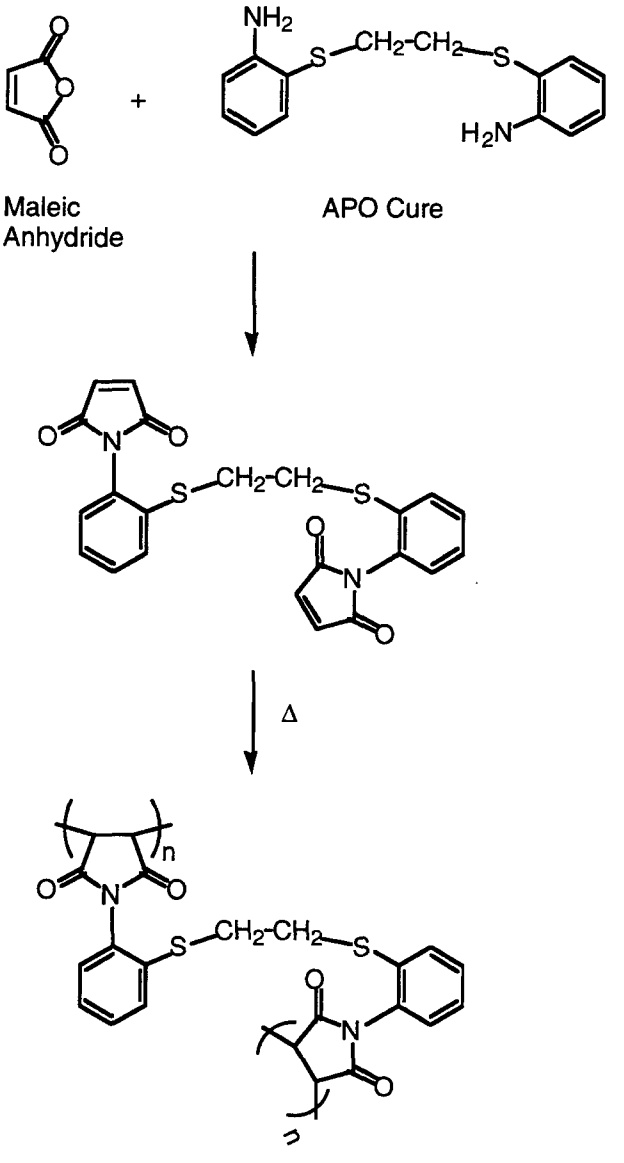

Figure 3. APO-BMI chemistry.

Surface tension forces drive the fluid resin to the contact points of the GMB, as observed in Figure 4 (an APO-BMI fracture surface) where it is most needed to bind the microspheres. The arrow marked A shows the resin "wicked" into the interstices of the GMB. Adhesion of the GMB is provided only by the small amount of resin that wicks up at these contact points of the microspheres. It is this wicking action alone that yields a self-supporting structure. The circular feature identified by the arrow marked B is the resin left behind after a GMB particle has de-bonded. Adhesion of the GMB is obviously poor as many of the microspheres exhibit these small disk shaped features. The feature identified by the arrow marked C is the debris remaining after a microballoon has fractured. Large areas of the fracture surface show little evidence of broken GMB, suggesting that the weak adhesion forces between the microspheres and the resin govern the aggregate strength of the structure, rather than the strength of the GMB themselves. Thus, the resulting solid

consists of a relatively weak, low-density structure, the properties of which are governed largely by the resin distribution around the contact points of the GMB and, to a lesser extent, by the inherently brittle glass microballoons.

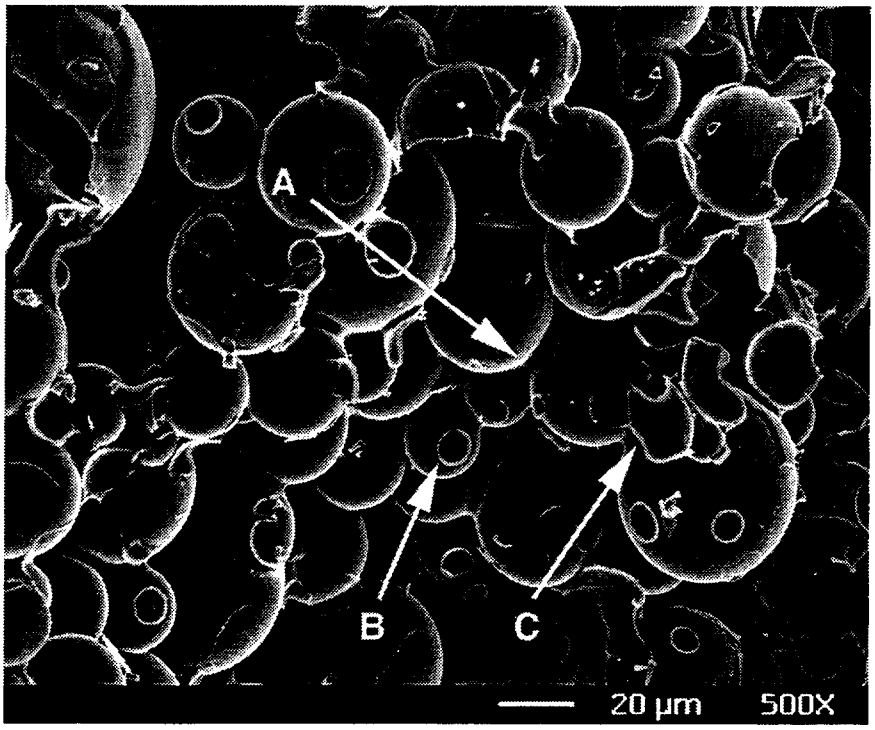

Figure 4. SEM image of fracture surface of APO-BMI foam. Arrow A shows the resin "wicked" into the interstices of the GMB. The circular feature at B is the resin left behind after a GMB particle has de-bonded. Arrow C points to the debris remaining after a microballoon has fractured.

TEPIC

In formulating TEPIC, our approach was to combine chemistries known to form thermally stable products. The two general reactions we used in our foam formulation are shown in Figures 5 and 6. The principal chemical reactants include an isocyanate, an epoxy and a catalyst. A surfactant is present only as a processing aid and does not react chemically. The GMB is added to adjust the density and modulus as a non-reactive filler. However, surface hydroxyls on the GMB may react with isocyanate forming a urethane linkage. The oxizolidinone shown in Figure 5 is formed by the reaction of an isocyanate and an epoxy. A cyclic isocyanurate (Figure 6) is formed by the trimerization of an isocyanate with a catalyst.

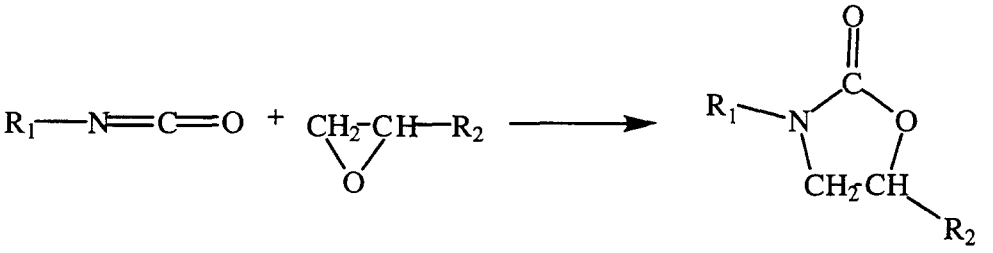

Figure 5. Oxizolidinone formation.

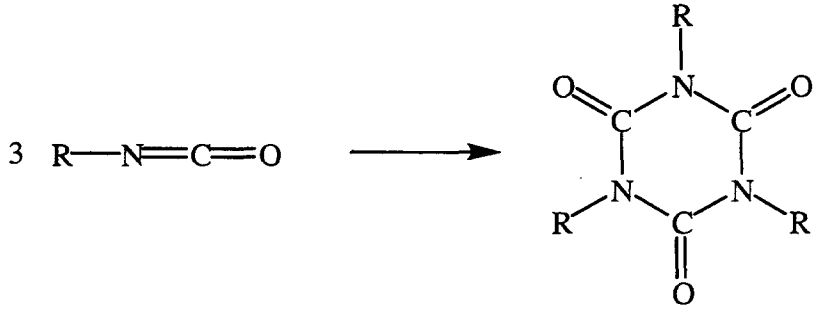

Figure 6. Isocyanurate formation.

Also, to increase mechanical integrity, we wanted the cell structure of the foam to resemble that of a traditional rigid polyurethane foam rather than that of APO-BMI. The resin matrix of polyurethane foams forms a continuous network of cell struts and cell walls (for closed cell foams). In such materials the mechanical properties are governed by the response of these struts and cell walls rather than by the minimal adhesion of the GMB in the APO-BMI structure. Figure 7a shows the typical structure of a TEPIC foam having a density of 0.42 g/cm^3. In this figure, the continuous polymer network is clearly defined. The large pores result from the entrapped air bubbles and some CO_2 produced from water (present as an impurity) reacting with the isocyanate. These air and CO_2 derived pores are distinguishable from the GMB in that they exhibit evidence of dimpling as they impinge on other nearby bubbles. The feature marked "A" is an example of an air or CO_2 derived pore. GMB, added to adjust density and stiffness, can be difficult to differentiate from these pores. In Figure 7b, several are identified as "B". These GMB show no evidence of dimpling. Rather, they are quite spherical and generally featureless. It is also apparent that, at the higher magnification of Figure 7b, the GMB particles exhibit evidence of de-bonding from the surrounding matrix. Quantitative size distribution analysis of the pores indicates that the gas derived bubbles have an average diameter of 70 μm while the GMB average 33 μm in diameter.

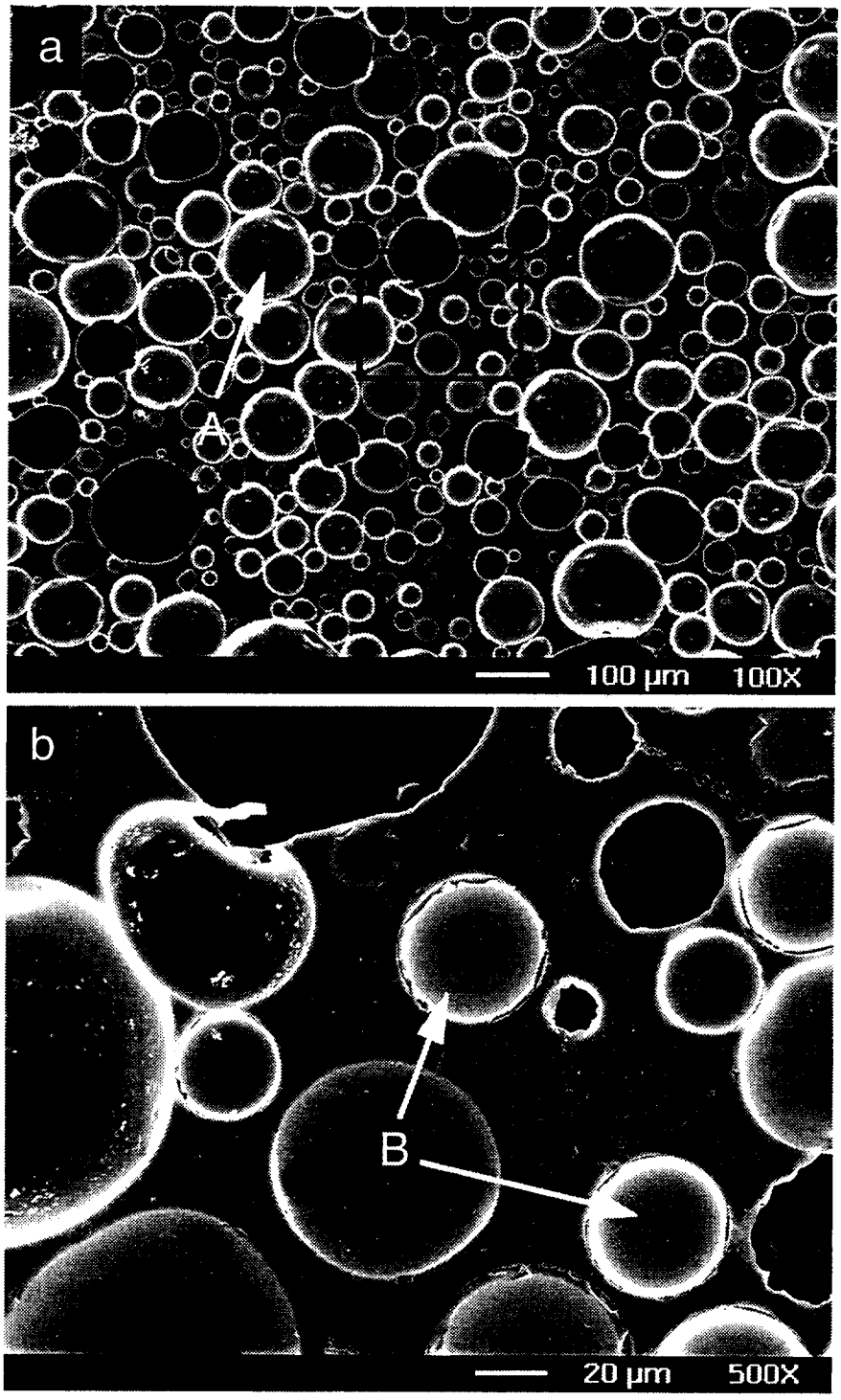

Figure 7. a) SEM image of TEPIC (ρ = 0.42 g/cm^3). Dimpled pores (A) are air or CO_2 derived bubbles. b) High magnification of region highlighted in 7a. Featureless spheres (B) are GMB which show evidence of debonding from the polymer matrix.

During the development of TEPIC many variables were examined and optimized. Much of our efforts were directed at minimizing void size by changing processing parameters and formulation ratios. As shown in Figure 7, the macrostructure of TEPIC more closely resembles a polyurethane blown foam than the APO-BMI syntactic foams (Figure 4). Initial formulations were viscous and trapped large air bubbles upon mixing, resulting in voids larger than 2 mm. The concentration, size, and density of GMB in the formulation were varied in an attempt to decrease the starting viscosity of the mix. Only a decrease in loading fraction of GMB had a favorable impact on the viscosity. The relative concentrations of surfactant, isocyanate, and epoxy were also probed, but no benefit was observed over the initial formulation. Different fillers were also examined. Unfortunately, only higher density foams were obtained.

The gel and rise times were shorter than optimal. Initial catalyst levels made the mixture start to expand within a minute after removal from the mixing blade. This short processing time resulted in a few, larger pores. Two obvious variables to examine were the catalyst level and specie. Decreasing the amount of catalyst should slow the gel (and rise) reaction so that the viscosity would increase slowly. By suppressing early gellation, the amount of mechanically trapped air was expected to be reduced, yielding a more uniform distribution of pore sizes. Several experiments were performed in order to determine the minimum concentration of TMR-3 and still have acceptable processing characteristics. The final catalyst level, indicated in Table 1, was high enough to give a uniform product and low enough to allow mixing and transfer before substantial expansion and gellation occurred. With regard to the selection of catalyst, TMR-3 is common in the reaction injection molding (RIM) industry and is already the slowest trimerization catalyst commercially available.

One final issue with respect to the effect of catalyst on processing, is the sequence in which it is added to the mix. In order to delay gellation as long as possible, we add it last after incorporation of the isocyanurate. This is contrary to conventional polyurethane foam processing, where the catalyst is added before the isocyanurate.

The previously discussed variables were limited by the processing of the foams. For example, if one wanted to produce to a lower density foam, all that is needed is to add more GMB or water to act as a blowing agent. However, more GMB makes the mix too thick and leads to non-uniform mixing by traditional techniques and additional water causes the foam to collapse before gelling. Alternatively, to formulate the foam so that it reacts more slowly, one would normally cut back on the catalyst. Unfortunately, we are already adding very little catalyst. Adding less would lead to uniformity and reproducibility concerns. After many attempts, a final TEPIC foam processing procedure was defined for the particular programmatic need. This final procedure is discussed in the previous Experimental Section and produces the 20 Kg billet shown in Figure 8.

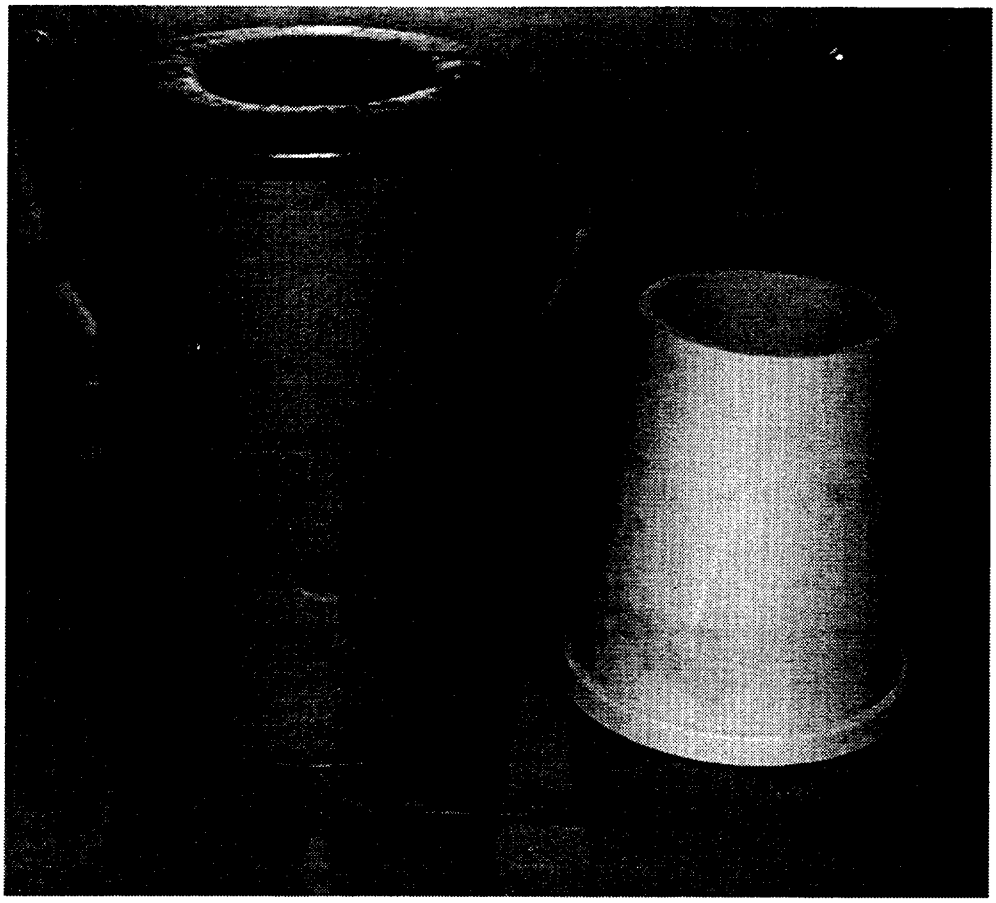

Figure 8. A 20 kg billet of TEPIC and a partially machined part.

Although water is not explicitly added to the TEPIC foam formulation, we believe that residual water, present in the GMB, polyol and surfactant, contribute significantly to the expansion of the foam during processing. The remaining foam expansion results from thermal expansion of entrapped air whipped into the resin during mixing.

Mechanical Properties of Foams

Quasi-static tension/compression results for TEPIC, 25°C

All specimens tested under quasi-static conditions had a density of 0.42 g/cm^3. Figure 9 shows the room temperature tensile behavior of TEPIC. While there is no specific performance requirement for the foam in tension, it is useful to characterize its tensile behavior, since failure invariably occurs due to the initiation and propagation of cracks in regions of local tension. Further, tensile strength bears directly on the machineability and handling characteristics of the foam. The foam behaves in a completely brittle manner in tension, exhibiting no plastic deformation at all up to the point of fracture. The modulus (defined as the slope of the linear loading portion of the stress strain curve) is approximately

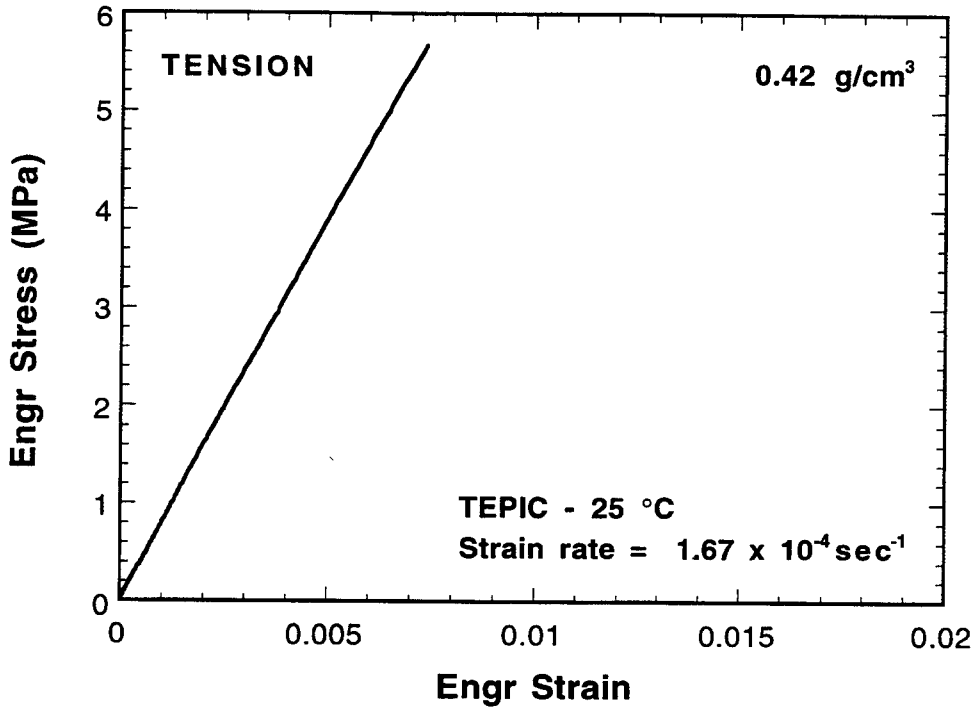

Figure 9. Tensile behavior of TEPIC. Foam loads in a linear manner and then fails without yielding.

770 MPa while the ultimate tensile strength of the foam is approximately 5.6 MPa (1 MPa = 145 psi). The energy absorption of the foam was derived from the area under the stress-strain curves as described above and found to be 0.021 J/cm^3. This is a low value and reflects the brittle nature of the foam. In comparison, a less brittle polyurethane foam of the same density exhibits a toughness value in tension that is 5 - 10 times greater than that of TEPIC.[10]

Figure 10 shows the room temperature compression behavior of TEPIC. The foam exhibits a well-defined initial linear loading regime. The modulus of the foam in compression is very nearly equal to that in tension, 790 MPa. Fracture occurs immediately after the loading curve begins to deviate from linearity at a crush stress, σ_{cr} = 20 MPa. This too is unlike a conventional polymeric foam, which exhibits a broad plateau stress subsequent to linear loading. In such foams, the plateau stress is associated with the controlled and reversible buckling of the cell wall and strut elements of the foam microstructure. TEPIC is sufficiently brittle that no such microstructural buckling can be accommodated. Rather the material fractures irreversibly and catastrophically. Not withstanding the brittle nature of the foam, the crush strength significantly exceeds the required value of 6.9 MPa. Because of its brittle behavior, the toughness of TEPIC in compression is low (compared to more conventional foams), approximately 0.40 J/cm^3.

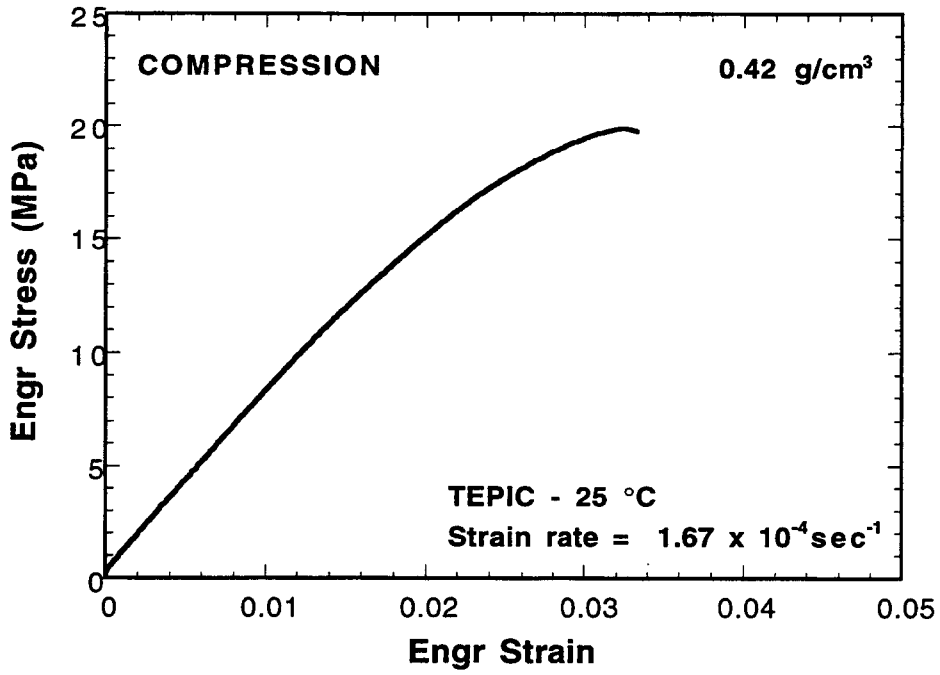

Figure 10. Compression behavior of TEPIC. The foam prior to failure can sustain very little non-linear loading.

The similarities in the mechanical response of the foam to tension and compression testing is shown in Figure 11 where the stress-strain curves from the previous two tests are plotted on the same axis scales. The curves essentially overlay until the point of tensile failure. Testing in compression simply suppresses the initiation and propagation of the cracking that leads to tensile fracture at very low strains.

Quasi-static tension/compression results for TEPIC, 200°C

Compression tests were performed on TEPIC at 200°C (Figure 12). The modulus of the foam at 200°C is 650 MPa, about 15% less than that at 25°C. Although measurably weaker than at 25°C, the crush strength of the foam is approximately 12 MPa and still exceeds the performance requirement.

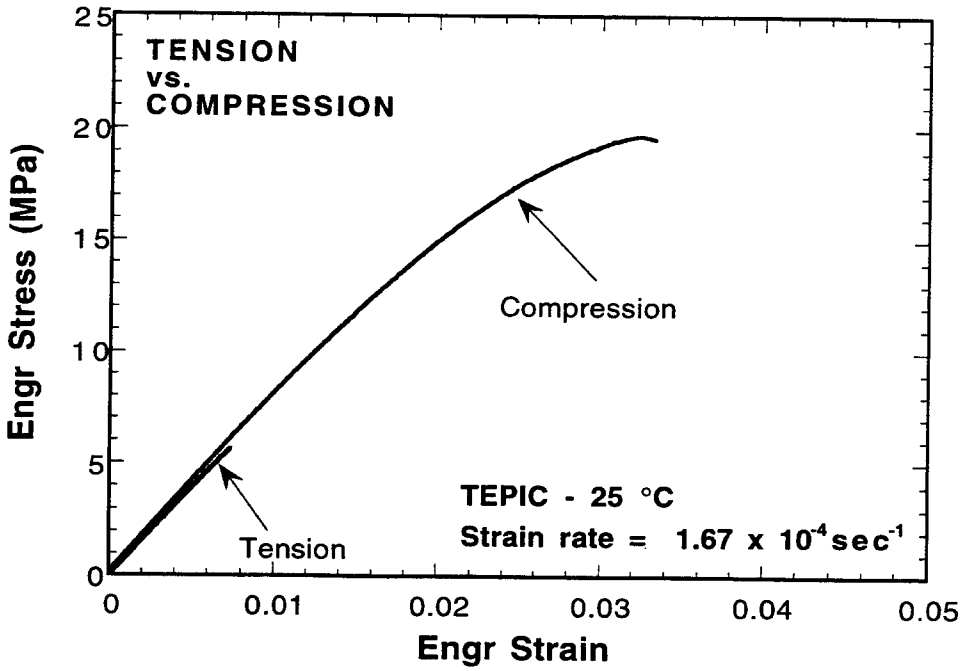

Figure 11. Comparison of the tension and compression behavior of TEPIC. Compression trace overlays a companion tension test up to the point of tensile failure.

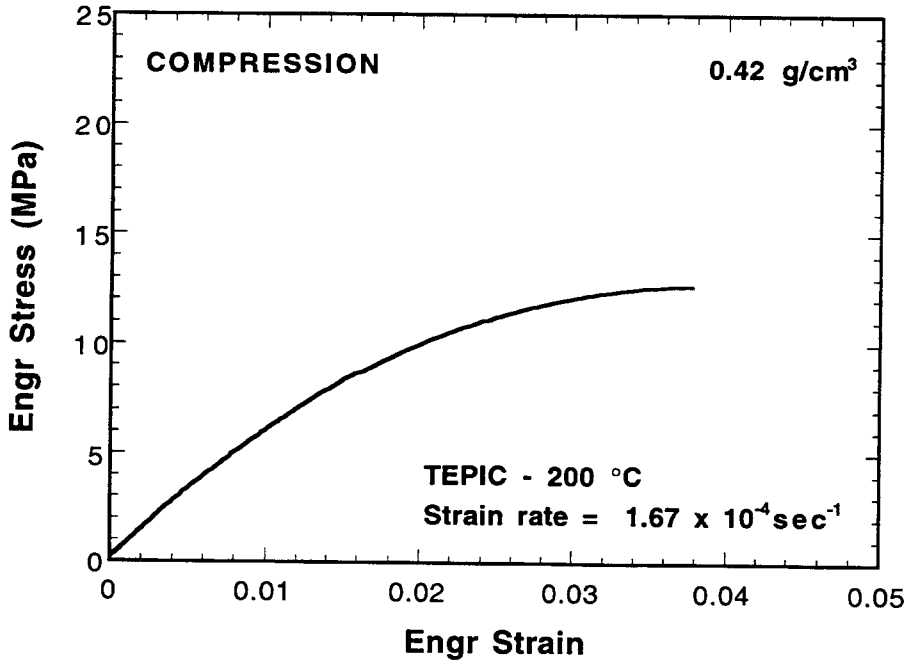

Figure 12. Compression stress-strain curve for TEPIC at 200 °C.

Comparison of TEPIC Properties to APO-BMI

In the application of interest, APO-BMI is used at a density 0.3 g/cm^3. Below we compare the properties of TEPIC at 0.42 g/cm^3 to APO-BMI at this lower density. For the quasi-static test results presented in Figures 13 - 15, the density of the APO-BMI specimens was 0.29 g/cm^3. Figure 13 shows that both materials are extremely brittle in tension. TEPIC has nearly six times the tensile strength of APO-BMI. The very low tensile strength of APO-BMI is reflected in its poor handling and machining characteristics. In thin sections, APO-BMI is extremely fragile and machined parts are easily damaged. TEPIC, in contrast, has superior handling and machining characteristics due to its higher strength.

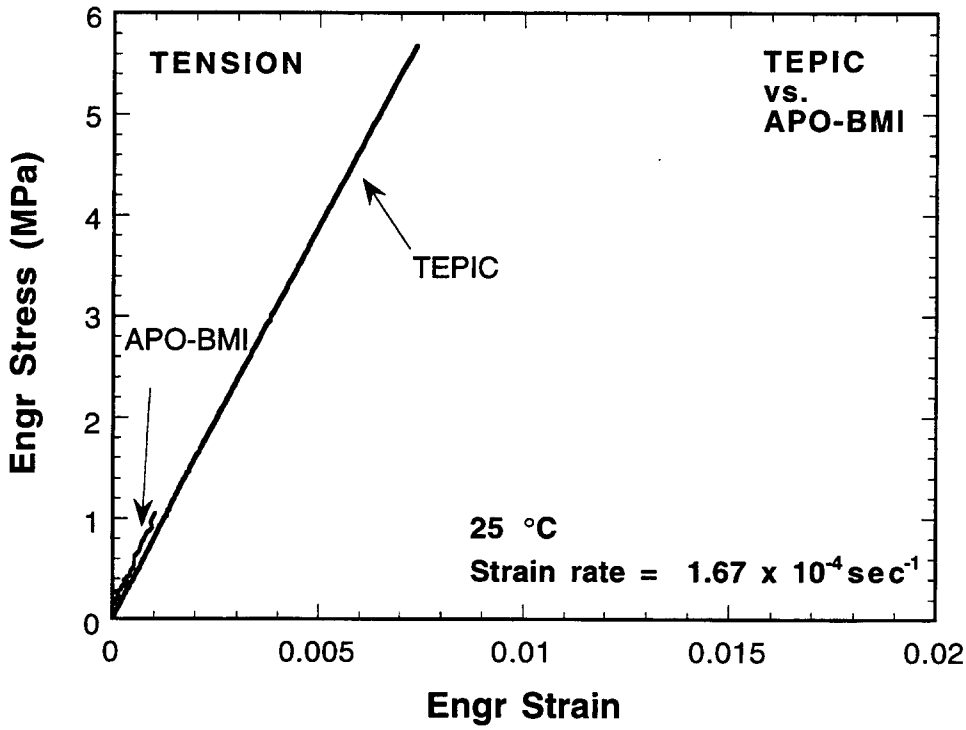

Figure 13. Comparison of tensile behavior TEPIC and APO-BMI at 25°C.

Figure 14 compares the compression behavior of TEPIC to APO-BMI. It is clear from the figure that while both materials exceed the performance requirements, TEPIC affords a substantial margin.

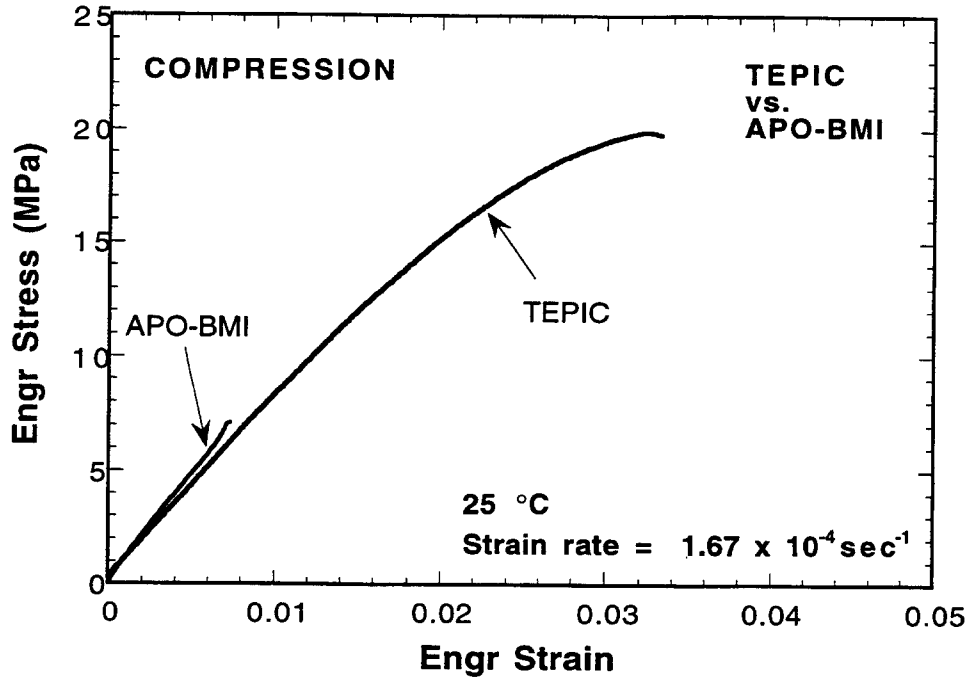

Figure 14. Comparison of compression behavior TEPIC and APO-BMI at 25°C.

Figure 15 compares the compression behavior of TEPIC to APO-BMI at 200°C. As in the room temperature tests, TEPIC significantly exceeds the performance requirements established for the foam.

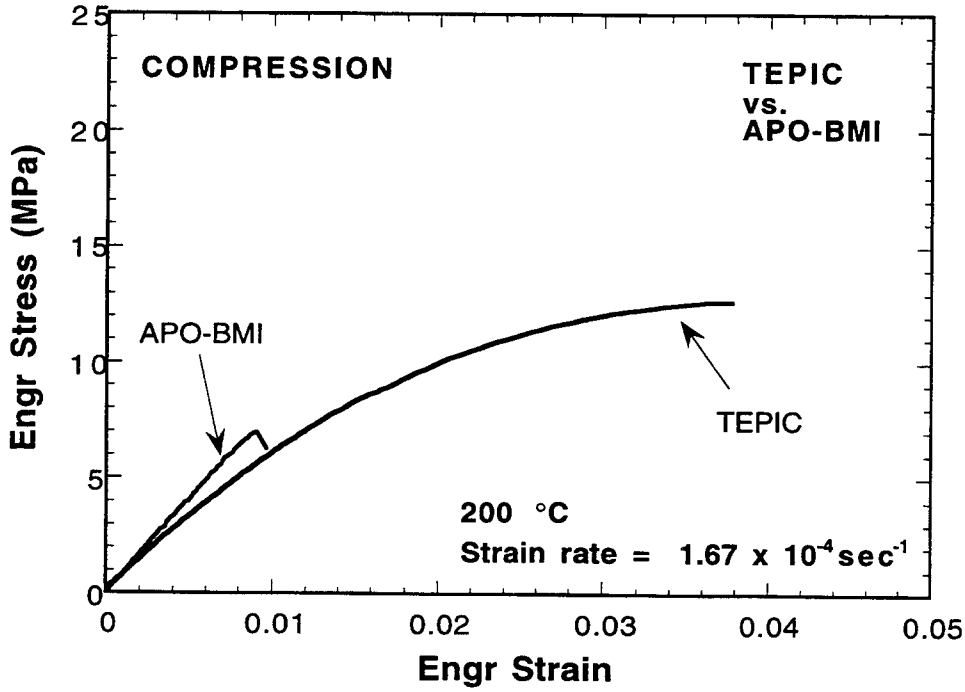

Figure 15. Comparison of the compression behavior of TEPIC and APO-BMI at 200°C.

Impact Properties of TEPIC/APO-BMI

For the envisioned application, a successful replacement foam for APO-BMI must have comparable impact properties and energy absorption characteristics. A series of tests were conducted to compare these properties. Figure 16 compares the impact characteristics of TEPIC and APO-BMI when tested at an incident strain rate of 90 sec^{-1} (impact velocity = 4.5 m/sec). The figure shows both the stress-strain curves (solid lines) as well as the

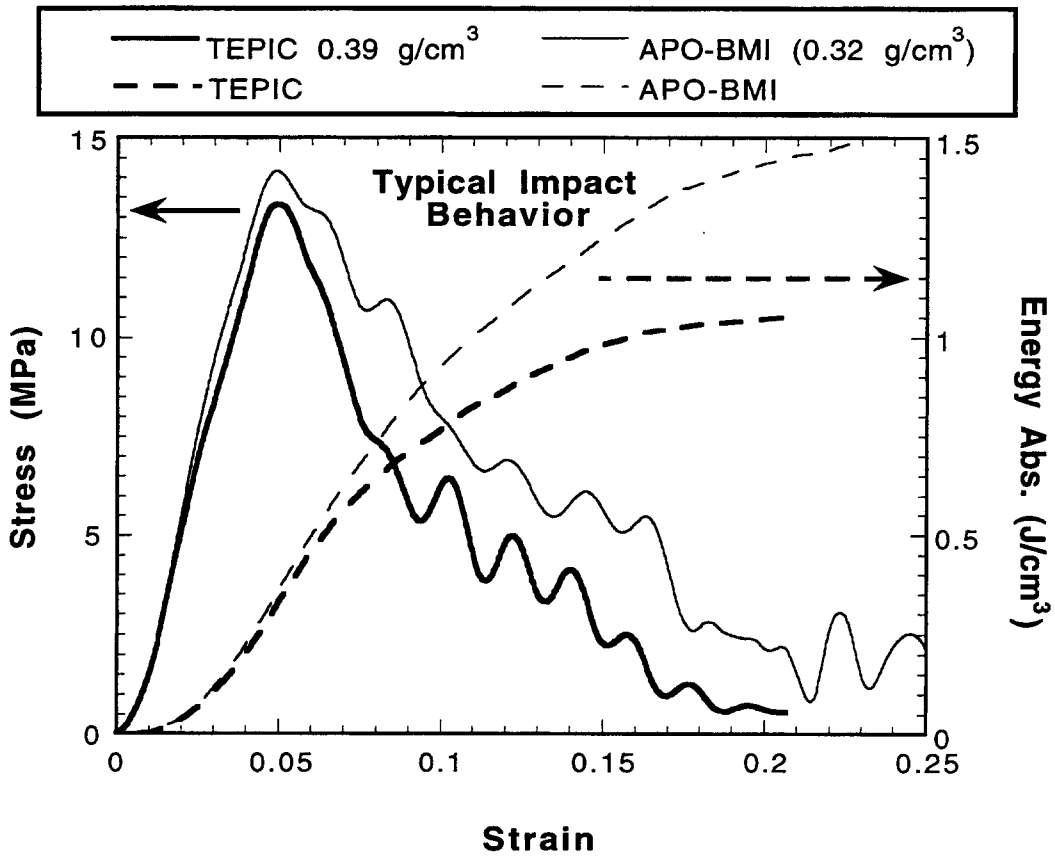

Figure 16. Comparison of the impact behavior of TEPIC (bold curves) and APO-BMI (fine curves) at 25°C.

cumulative energy absorption (broken lines) as a function of strain for both foams. Note that the density of the two foams are not the same since APO-BMI was only available at densities near 0.3 g/cm^3. Failure of the specimens is defined as the maximum stress and it is meaningful to compare the material response only up to this point. Up to the point of failure, the behaviors of both materials are virtually identical in terms of both the mechanical loading as well as the energy absorption characteristics. Beyond this point, their behavior diverges. These differences reflect only the way in which the foams crush. TEPIC tends to catastrophically fracture into large sections that are ejected from under the impactor. As such the load falls off very rapidly and the energy absorption plateaus quickly. APO-BMI tends to crush down upon itself. Because of this, there is more

residual material beneath the impactor, and the load tends to fall off more gradually. Neither material, however, has any significant physical integrity beyond the peak stress and can no longer be considered structural.

Figure 17 summarizes the energy absorption characteristics of the two foams as a function of density at room temperature. The comparison is limited due to the narrow range of densities for APO-BMI. The data is plotted verses normalized density (ρ^* is the measured density of each specimen and ρ_s is the density of the solid constituents). The figure shows the expected trend of increasing energy absorption with increasing density for TEPIC. Notwithstanding the scatter in the data, it is clear from Figure 17 that TEPIC can be prepared with impact properties that are equivalent or superior to those of APO-BMI.

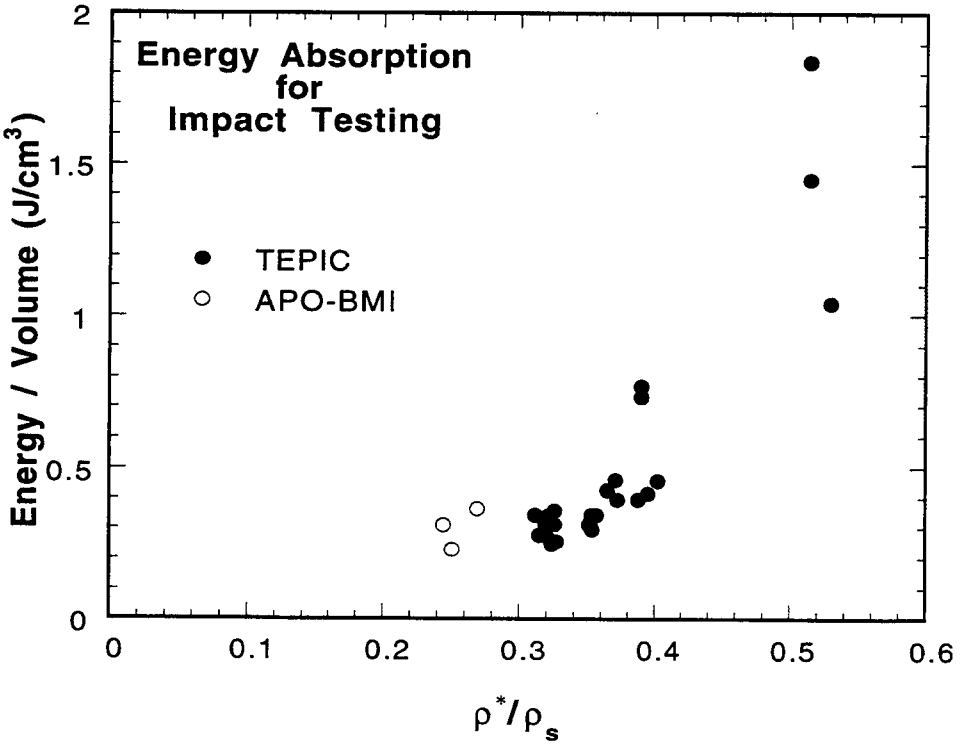

Figure 17. Summary of energy absorption characteristics for TEPIC and APO-BMI at 25°C.

Strain Rate Effects on Mechanical Properties of TEPIC

The mechanical properties of polymeric foams can be strongly influenced by strain rate. Because of the anticipated mechanical environment, it was necessary to assess the effect of strain rate on both modulus and strength. This was done through a series of compression tests performed over seven orders of magnitude in strain rate as described in the Experimental Section using different testing instruments.

Figure 18 shows a typical stress-strain curve generated using the servomechanical test frame. The imposed strain rate is about one-half that of that shown in Figure 11 and not

surprisingly, the two compression curves are quite similar. As in Figure 11, the foam specimen tested in Figure 18 shows a well-defined modulus slope. Once again, brittle failure occurs catastrophically, shortly after the loading slope begins to deviate from linearity.

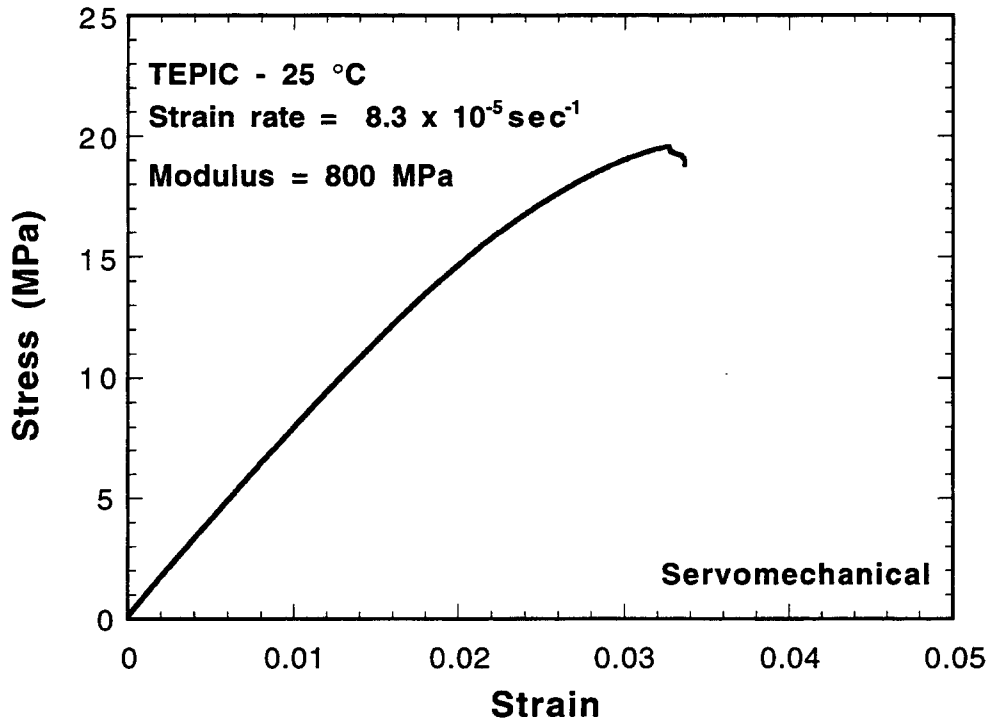

Figure 18. Stress-strain curve for TEPIC tested at 8.3 x 10^{-5} sec^{-1} in displacement control.

Figure 19 shows the stress-strain curve for a specimen tested in the servohydraulic test apparatus at two orders of magnitude higher strain rate. The curve is nearly identical to that shown in Figure 18 reflecting the minimal effect of strain rate on mechanical properties as well as the consistency between instruments. Only the crush strength is somewhat higher than that shown in Figure 17.

Figure 20 shows the stress-strain curve generated under impact conditions. The "tail-in" at small strains results from the absence of a mechanically attached extensometer. For this test, the modulus is computed as maximum slope of the stress-strain curve.

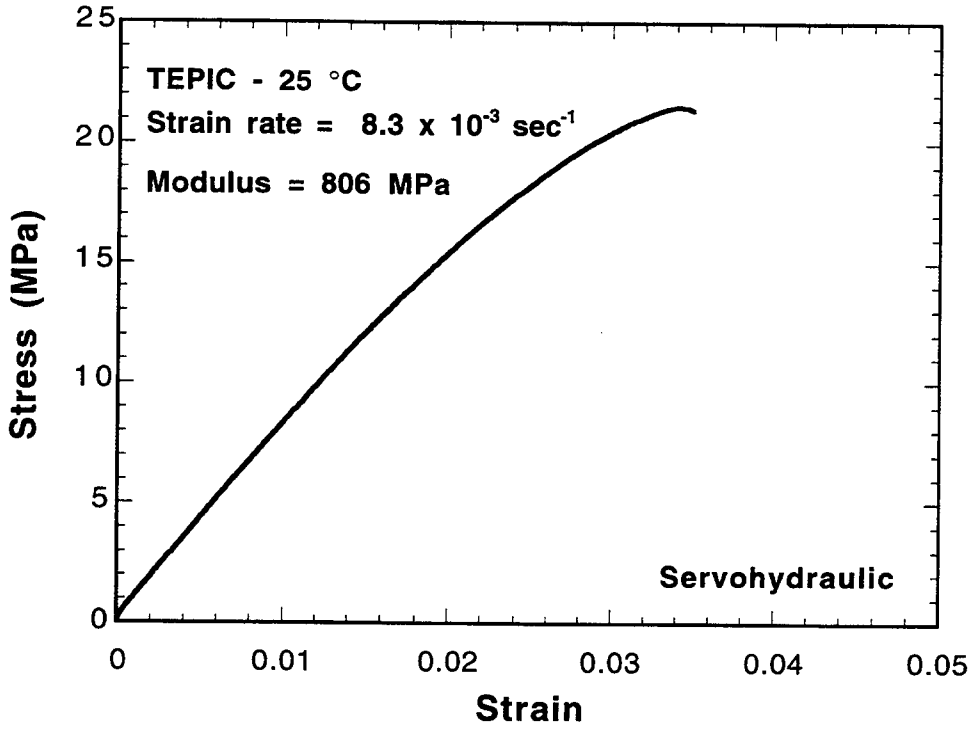

Figure 19. Stress-strain curve for TEPIC tested at 8.3 x 10^{-3} sec^{-1} in displacement control.

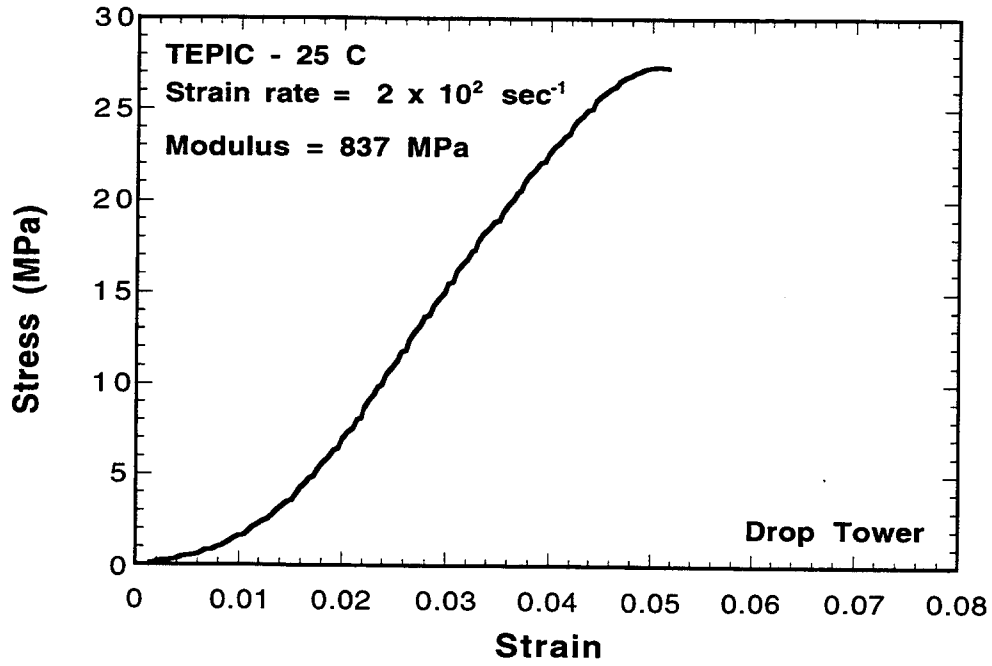

Figure 20. Stress-strain curve for TEPIC at 2.0 x 10^{2} sec^{-1} under impact conditions.

Figure 21 shows the strain rate dependence of the foam modulus over the entire range of rates examined. Each modulus measurement is identified by the test apparatus used. It is clear from Figure 22 that there are no systematic differences in the modulus values derived from the different test instruments.

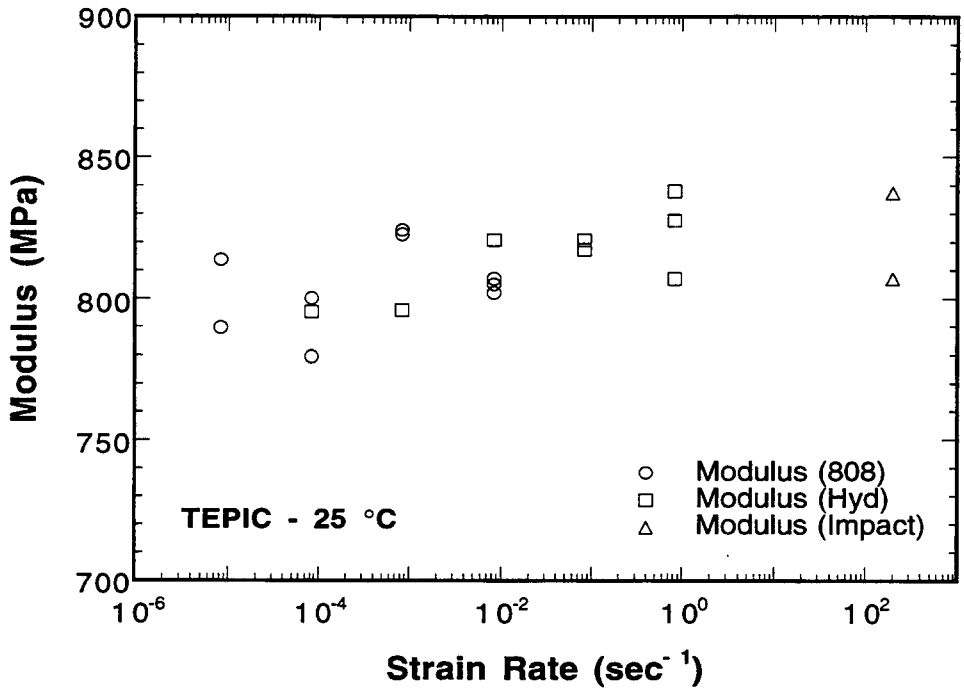

Figure 21. Moduli derived from all compression tests.

Figure 22 shows the average modulus at each strain rate and reveals that that the modulus is only weakly dependent on the imposed strain rate. A power-law relationship of the form:

$$E^* \propto \dot{\varepsilon}^n$$

can be fit to the data yielding a strain rate exponent, n, of 0.002.

Figure 23 shows the strain rate dependence of the crush strength. For this data, the strength is considerably more sensitive to the imposed strain rate. A power law expression is fit to this data as well, yielding a strain rate exponent of n = 0.021. In this case, however, empirical expressions, other than the simple power law form, might capture the rate sensitivity more accurately.

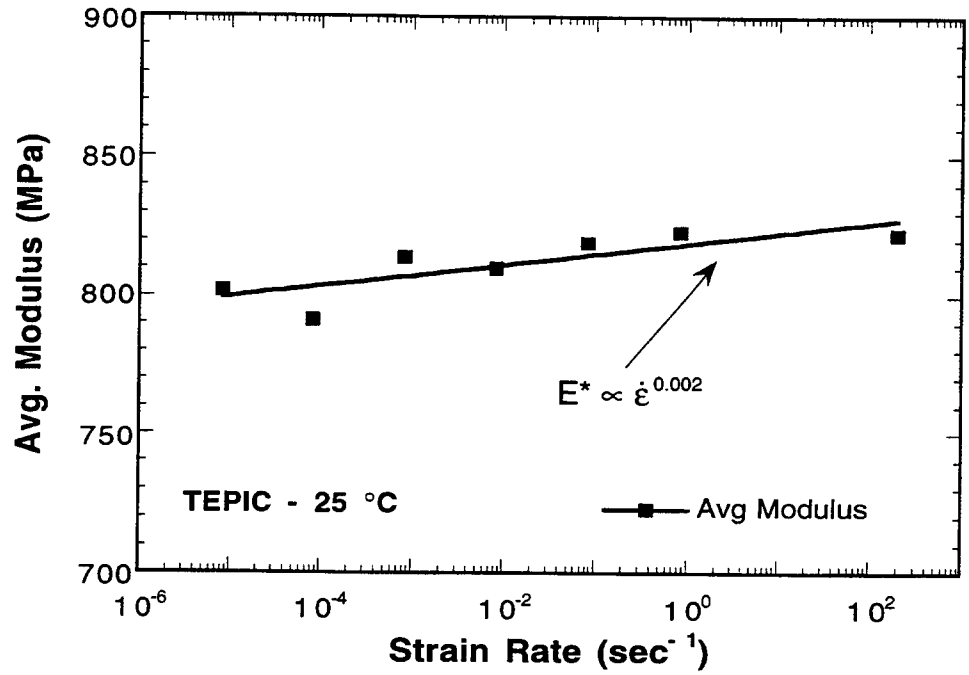

Figure 22. Average moduli at each strain rate. Data is fit to a power-law expression yielding a strain rate exponent of 0.002.

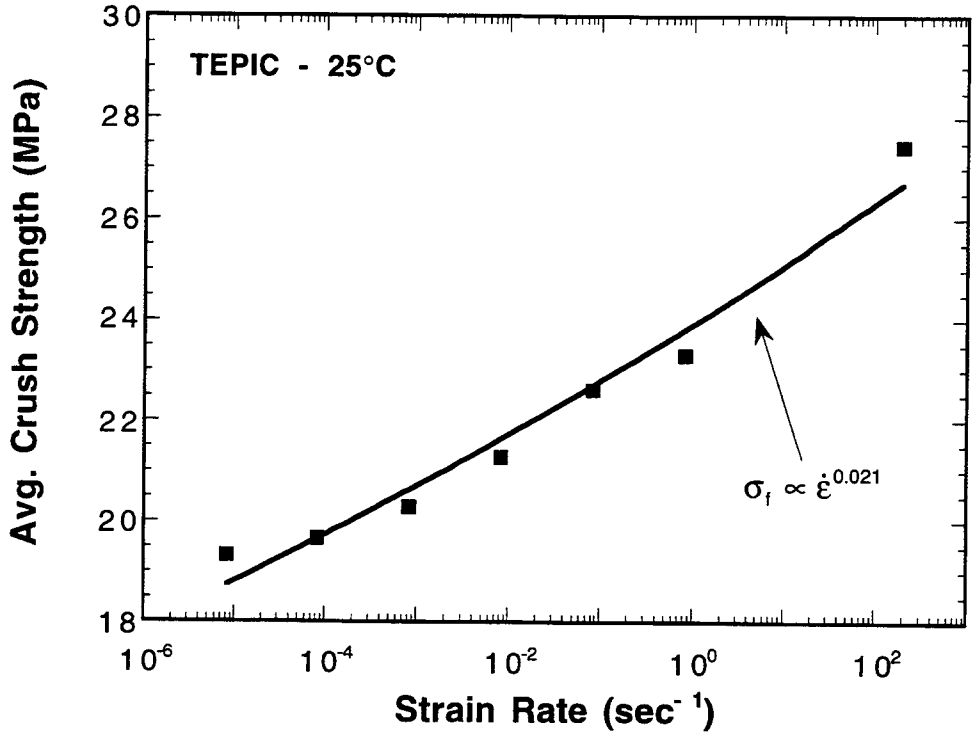

Figure 23. Average strength at each strain rate. Data is fit to a power-law expression yielding a strain rate exponent of 0.020.

Table 2 summarizes the data presented in Figures 22 and 23. It also summarizes strain rate dependence of the energy absorption of the foam. Because the modulus change is so small with increasing strain rate, the toughness of the foam scales directly with the influence of strain rate on the crush strength of the material.

Table 2. Effect of strain rate on compression properties of TEPIC.

Strain Rate (s^{-1})	Modulus (MPa)	Crush Strength (MPa)	Energy Absorption (J/cm^3)
2.0×10^{-2}	823	27.5	1.04
8.3×10^{-1}	822	23.3	0.45
8.3×10^{-2}	819	22.6	0.47
8.3×10^{-3}	810	21.3	0.43
8.3×10^{-4}	814	20.3	0.40
8.3×10^{-5}	791	19.6	0.39
8.3×10^{-6}	802	19.3	0.36

IV. CONCLUSIONS

TEPIC foams meets or exceeds all requirements necessary to replace APO-BMI in structural applications. With respect to formulation, processing and microstructural considerations, none of the foam constituents have been identified as human carcinogens, the formulation can be scaled to large batch sizes, and the cured foam has been demonstrated to be easily machined into complex shapes. Because the foam has higher strength (especially in tension) and no voids greater than 2 mm in diameter, parts having thin sections can be successfully machined, handled and assembled. This is the main advantage of TEPIC foams over their APO-BMI counterparts - they are more readily handled, leading to less breakage and fewer defective parts.

With respect to specific mechanical properties, TEPIC exceeds both the stated requirements (6.9 MPa compressive strength at 200°C) as well as the mechanical performance of APO-BMI. Crush strength at 25°C is approximately 20 MPa, while at 200°C it is 13 MPa. These strength levels are realized at a foam density of $\approx$ 0.4 g/cm^3, well below the maximum allowable density of 0.6 g/cm^3.

The present principal limitation is the narrow density range for TEPIC foams. Work is underway to expand the available range of density while maintaining the machineability, handling and mechanical property characteristics.

REFERENCES

1. D. R. Jamieson, Final Report, Allied Signal-Kansas City Division, BDX-613-1480, **1977.**
2. D. R. Jamieson, Topical Report, Allied Signal-Kansas City Division, BDX-613-1854, **1977.**
3. A. Young, Topical Report, Allied Signal-Kansas City Division, BDX-613-1886, **1977.**
4. D. A. Spieker, Final Report, Kansas City Division, KCP-613-4848, **1992.**
5. D. R. Jamieson, Final Report, Allied Signal-Kansas City Division, BDX-613-2713, **1983.**
6. D. R. Jamieson, Final Report, Allied Signal-Kansas City Division, BID-A032, **1980.**
7. D. R. Jamieson, Topical Report, Allied Signal-Kansas City Division, BDX-613-3476, **1986.**
8. D. J. Wolfe, Final Report, Allied Signal-Kansas City Division, BID-A656, **1980.**
9. G. Oertel, Polyurethane Handbook, 2nd Edition, Hanser Publishers, New York, **1994.**
10. S. H. Goods, C. L. Neuschwanger, C. Henderson and D. M. Skala, J. Appl. Polymer Sci., 68:1045, **1998**

DISTRIBUTION:

5 Hewlett-Packard Company
Attn: Cari Neuschwanger
1501 Page Mill Road, MS 5L-C
Palo Alto, CA 94304-1126

4 Allied Signal, Inc.
Federal Manufacturing & Technologies Division (FM&T)
Attn: George McEachen
Dave Spieker, D/MB3 2C43
E. Grotheer, D/MB3 2C43
Patricia Wilson
P. O. Box 419159
Kansas City, MO 64141-6159

2 Los Alamos National Laboratories
Attn: J. E. Coons, MS C930
C. G. Sandoval, MS F602
P. O. Box 1663
Los Alamos, NM 87545

2 Lawrence Livermore National Laboratory
Attn: J. D. LeMay, L-092
G. B. Balazs, L-092
P. O. Box 808
Livermore, CA 94550

1 Martin Energy Systems
Oak Ridge National Laboratory
Attn: Lisa Thompson
P. O. Box 2008
Oak Ridge, TN 37831-6285

1 Atomic Wapons Establishment
Attn: Norman R. Godfrey
Aldermaston
Reading, Berks
England RG74PR
UNITED KINGDOM

1	MS0367	R. S. Saunders, 1815
1	MS0367	P. B. Rand, 1815
1	MS0443	M. K. Neilsen, 9117
1	MS0834	A. M. Kraynik, 9112
1	MS0834	M. L. Hobbs, 9112
1	MS0925	R. L. Myers, 1472
1	MS0958	C. J. Adkins, 1472
1	MS0958	J. A. Emerson, 1472
1	MS0958	M. W. Donnelly, 1472

1	MS0958	T. R. Guess, 1472
1	MS0961	J. A. Sayre, 1403
1	MS1407	J. H. Aubert, 1815
1	MS1407	R. J. Salzbrenner, 1805
1	MS1407	T. A. Ulibarri, 1811
3	MS9021	W. Carter, 8815
1	MS9036	D. Neustel, 2254
1	MS9036	M. Hinkley, 2254
1	MS9042	D. Handrock, 8742
1	MS9042	W. Y. Lu, 8746
1	MS9102	M. Perra, 8402
1	MS9403	M. I. Baskes, 8712
1	MS9403	M. L. Tootle, 8712
10	MS9403	S. H. Goods, 8712
1	MS9405	C. Henderson, 8230
1	MS9405	D. Skala, 8230
1	MS9405	J. M. Hruby, 8230
1	MS9405	L. Domeier, 8230
10	MS9405	L. Whinnery, 8230
1	MS9405	P. Kiefer, 8230
1	MS9405	T. M. Dyer, 8700
	MS9042	Attn: E-R Chen, 8742
	MS9042	G. J. Thomas, 8715
	MS9042	W. A. Kawahara, 8746
	MS9043	J. C. F. Wang, 8713
	MS9161	K. L. Wilson, 8716
	MS9161	S. M. Foiles, 8717
	MS9402	C. M. Hartwig, 8701
	MS9405	P. N. Nielan, 8743
1	MS9420	L. A. West, 8200
	MS9133	Attn: B. Affeldt, 8210
	MS9409	C. Oien, 8260
	MS9409	G. Kubiak, 8250
	MS9430	A. J. West, 8240
	MS9430	L. N. Tallerico, 8204
3	MS9018	Central Technical Files, 8940-2
1	MS0899	Technical Library, 4916
1	MS9021	Technical Communications Department, 8815/ Technical Library, MS0899, 4916
2	MS9021	Technical Communications Department, 8815 for DOE/OSTI